Wireless Performance of a Fully Passive Neurorecording Microsystem Embedded in Dispersive Human Head Phantom

Helen N. Schwerdt, Junseok Chae
Electrical, Computer, and Energy Engineering
Arizona State University
Tempe, AZ, USA

Félix A. Miranda
Antenna and Optical Systems Branch
NASA Glenn Research Center
Cleveland, OH, USA

***Abstract*—This paper reports the wireless performance of a biocompatible fully passive microsystem implanted in phantom media simulating the dispersive dielectric properties of the human head, for potential application in recording cortical neuropotentials. Fully passive wireless operation is achieved by means of backscattering electromagnetic (EM) waves carrying 3rd order harmonic mixing products ($2f_0 \pm f_m$=4.4-4.9 GHz) containing targeted neuropotential signals ($f_m \approx$1-1000 Hz). The microsystem is enclosed in 4 µm thick parylene-C for biocompatibility and has a footprint of 4 mm × 12 mm × 500 µm. Preliminary testing of the microsystem implanted in the lossy biological simulating media results in signal-to-noise ratio's (SNR) near 22 (SNR≈38 in free space) for *millivolt* level neuropotentials, demonstrating the potential for fully passive wireless microsystems in implantable medical applications.**

I. Introduction

In order to advance wireless biomedical implant technology, the safety and durability of the internal electronics is of utmost importance. For cortical brain recording applications, potential hazards introduced by implanted circuitry severely limit their clinical manifestation. Fully passive circuitry may alleviate many of the risks related to heat dissipation and potential failure of internal power sources, regulators, and/or harvesters. The fully passive device, presented herein, excludes any integrated power sources and transmits targeted neuropotential signals wirelessly by means of microwave backscattering (Fig. 1).

Previous testing of the fully passive wireless microsystem demonstrated a sensitivity of ~500 µV$_{pp}$ (V_m) as recorded from a frog's sciatic nerve and bandwidth (f_m) of 5-2000 Hz [1], [2]. However, prior testing did not take into account the inhomogeneous tissue enclosing the microsystem in its intended application that would significantly alter penetrating EM signals.

II. Materials and Methods

Miniaturization of the on-chip implant antenna is achieved by use of an electrically small slot antenna operating at higher microwave frequencies. Additional onboard circuitry includes 3 MIM (Metal-Insulator-Metal) capacitors (1 bypass and 2 loading capacitors) and 2 off-chip varactors (Fig. 2(a)).

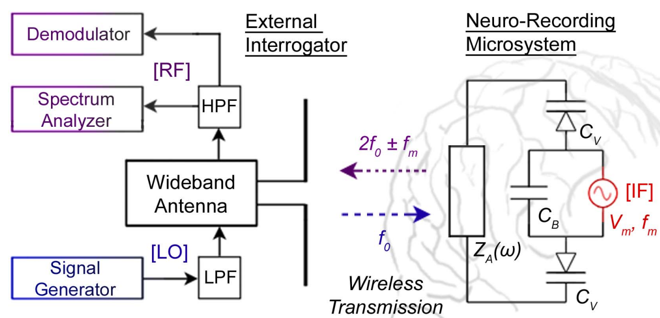

Figure 1. Simplified schematic of fully passive wireless operation. At the external interrogator (left), a signal generator supplies the f_0 local oscillator (LO) carrier that is low pass filtered (LPF) and wirelessly transmitted via wideband antenna to the microsystem (right) antenna ($Z_A(\omega)$), which then backscatters 3rd order harmonic RF signals ($2f_0 \pm f_m$). The RF signals are received by the external antenna and fed into a high pass filter (HPF) and demodulated to baseband (f_m).

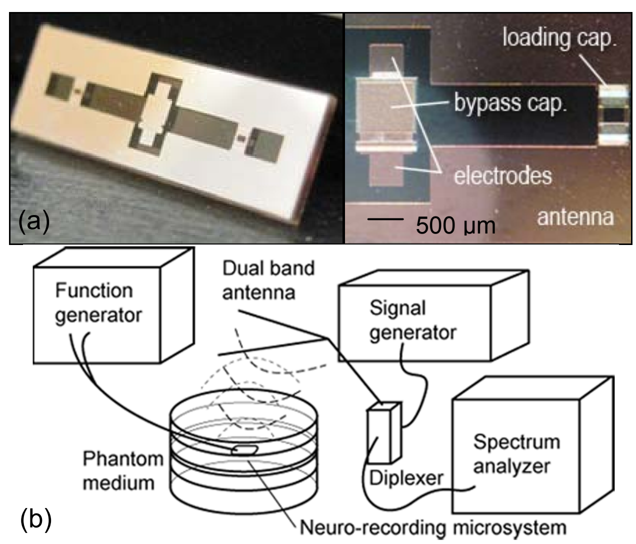

Figure 2. (a) Neurorecording microsystem (close up on right), measures 4×12×0.5mm^3 and integrates on-chip antenna, MIM capacitors, and electrodes connecting V_m input to varactors. (b) Setup for wireless testing as embedded in phantom medium.

Capacitive loading by fabricated MIM capacitors permits dual band operation at the incident frequency (f_0) and backscatter frequency ($2f_0 \pm f_m$). An external interrogator supplies the fundamental carrier ($P_0@f_0$) signal to activate the microsystem's mixing and backscattering functions. Varactors retrieve this induced carrier ($P_0@f_0$) along with the internal neuropotential ($V_m@f_m$) signals to generate 3rd order harmonic mixing products ($2f_0 \pm f_m$) that are then backscattered by the on-chip antenna to the external interrogator, where the neuropotential signal is recovered (Fig. 2(b)).

The phantom medium is composed of multiple strata mimicking the complex permittivity characteristics of skin, bone, dura, gray matter, and white matter layers of the average human head (Fig. 3) [3]. Open-ended coaxial probe measurements (85070D, Agilent) of the various phantom layers are performed to ensure their permittivity values closely correspond to the reported values for real human tissues (Fig. 4) [4].

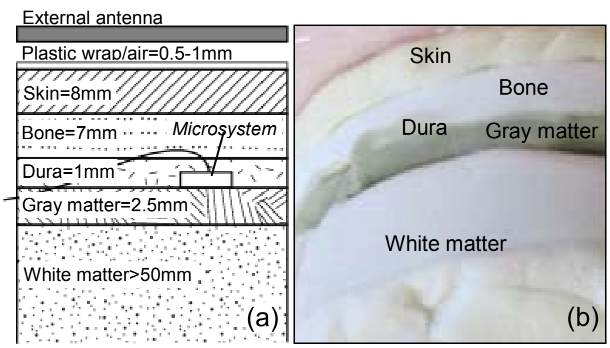

Figure 3. (a) Diagram of stratified human head phantom medium (with individual thicknesses) and (b) cross section of the phantom medium assembly.

During wireless testing, the neurorecording microsystem is embedded into the dura stratum of the phantom and the complete phantom is enclosed by plastic wrap to maintain an insulating barrier from the external interrogator (the external antenna is placed in direct contact with the plastic wrap for a total wireless separation of near 1 mm). Emulated neuropotential signals (V_m=0-50 mV$_{pp}$, f_m=5-1000 Hz), are applied to a twisted pair of insulated feed-through wires connected to the front of the microsystem. Local oscillator (LO) power (P_0=0-20 dBm) is supplied from a signal generator (8341A, HP) to supply the carrier. The SNR of the backscattered 3rd order harmonics ($2f_0 \pm f_m$) from the microsystem is quantified by the ratio between the amplitude of the $\pm f_m$ sidebands around $2f_0$ as visualized in the spectrum analyzer (E4448A, Agilent) with an average noise floor of -136 dBm (Fig. 5(a)). The average observed SNR for the three different types of microsystems (low resistivity silicon, high resistivity silicon, and glass substrates) tested in air and in the phantom medium are summarized in Fig. 5(b). The microsystem based on high resistivity silicon and glass substrates produced a SNR of greater than 20 dB inside the phantom, whereas devices based on low resistivity silicon fail to generate any wireless response. Future work will involve enhancing the sensitivity of the microsystem and minimizing noise in the external demodulator, as will be delineated in the full paper.

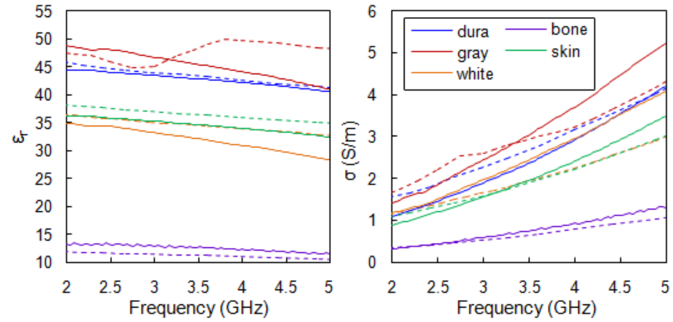

Figure 4. Plot of complex permittivity (ε_r) and conductivity (σ) for real (dashed) and measured phantom (solid) human head tissue lay

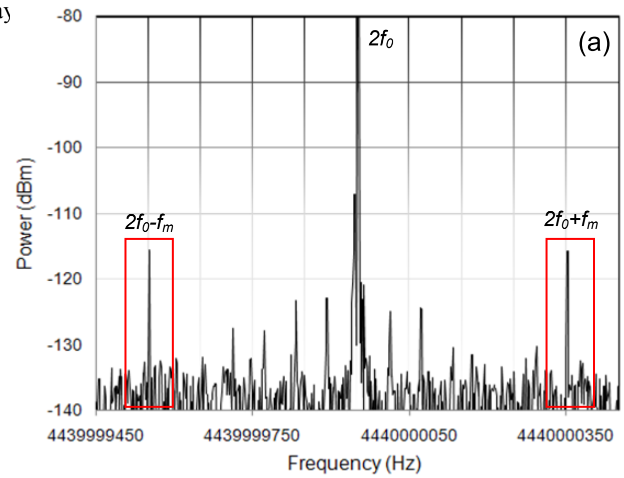

SNR	Free Space	Phantom
Low Resistivity Si	0	0
High Resistivity Si	38.9	22.0
Glass	36.6	21.3

(b)

Figure 5. (a) Spectral plot of wirelessly backscattered neuropotentials ($2f_0 \pm f_m$, labeled) from microsystem in phantom (V_m=50mV$_{pp}$, f_m=400 Hz). (b) SNR measurements for 3 different microsystem substrates.

ACKNOWLEDGEMENT

This work is supported in part by NSF (ECCS-0702227), NIH (5R21NS059815-02), and NASA Graduate Student Research Program (NNX09AK93H).

REFERENCES

[1] H.N. Schwerdt, W. Xu, S. Shekhar, A. Abbaspour-Tamijani, B.C. Towe, F.A. Miranda, and J. Chae, "A fully passive wireless microsystem for recording of neuropotentials using RF backscattering methods," *IEEE J. MEMS*, vol. 20, no. 5, pp. 1119-1130, Oct. 2011.

[2] A. Abbaspour-Tamijani, M. Farooqui, B.C. Towe,and J. Chae, “A miniature fully-passive microwave back-scattering device for short-range telemetry of neural potentials,” *Proc. Ann. Int. Conf. IEEE-EMBS,* Aug. 2008, pp. 129-132.

[3] K. Ito, K. Furuya, Y. Okano, and L. Hamada, “Development and characteristics of a biological tissue-equivalent phantom for microwaves.” *Electronics and Communications in Japan (Part I: Communications),* vol. 84, pp. 67–77, 2001.

[4] C. Gabriel. “Compilation of the dielectric properties of body tissues at RF and microwave frequencies.” *Report N.AL/OE-TR- 1996-0037,* Occupational and environmental health directorate, June 1996.

Wireless Performance of a Fully Passive Neurorecording Microsystem Embedded in Dispersive Human Head Phantom

Helen N. Schwerdt[1], Junseok Chae[1], Félix A. Miranda[2]

[1]School of Electrical, Computer, and Energy Engineering
Arizona State University, Tempe, Arizona, USA

[2]Antenna and Optical Systems Branch
NASA Glenn Research Center, Cleveland, Ohio, USA

2012 IEEE International Symposium on Antennas and Propagation
Chicago, Illinois, USA
July 9, 2012 (Session 156.2)

Outline

- Introduction
- Operation
  - Microsystem
  - Wireless Backscattering
- Fabrication
- Wireless Performance in Air
- Preparation of Phantom Emulating Human Head
- Wireless Performance in Phantom
- Conclusion & Future Work

Motivation

"Neurorecording" → recording neuropotentials

(ie. electrical activity originating from neural signaling in brain or other nervous systems)

Paraplegia/Paralysis	6 (USA)
Alzheimer's Disease	5.3 (USA)
Epilepsy	4 (USA), 50 (world)
Parkinson's Disease	1 (USA)

BrainGate BCI[3]

microsystem with wiring to head platform

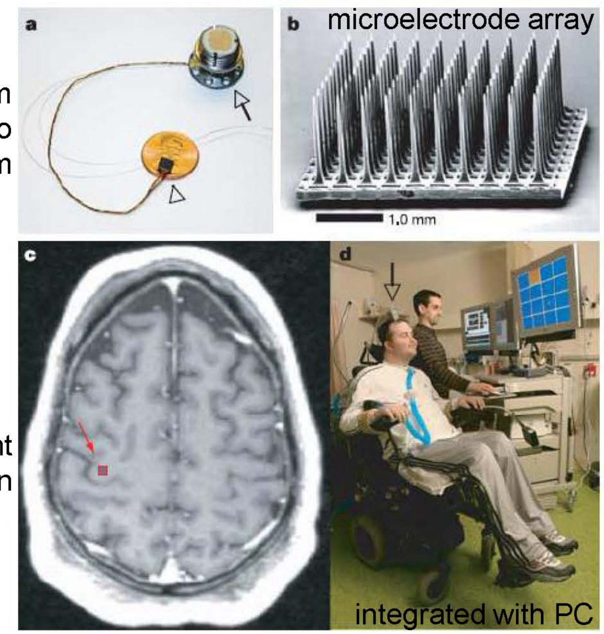

implant position

- Prosthetics & rehabilitation[3-5]
- Treatment
- Brain machine interfaces
- Advance understanding of brain
  - One of the least understood and most important organs
  - Most CNS knowledge based on conjecture

EEG scan of epileptic seizure

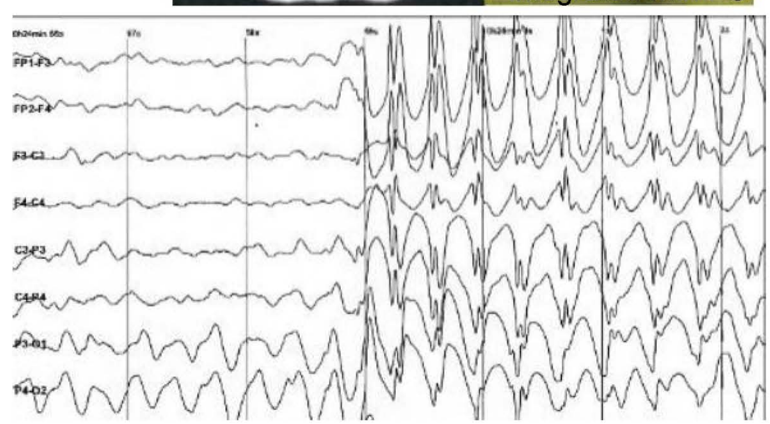

CNS = central nervous system

BCI = brain computer interface   *EEG* = electroencephalography

Current Recording Systems

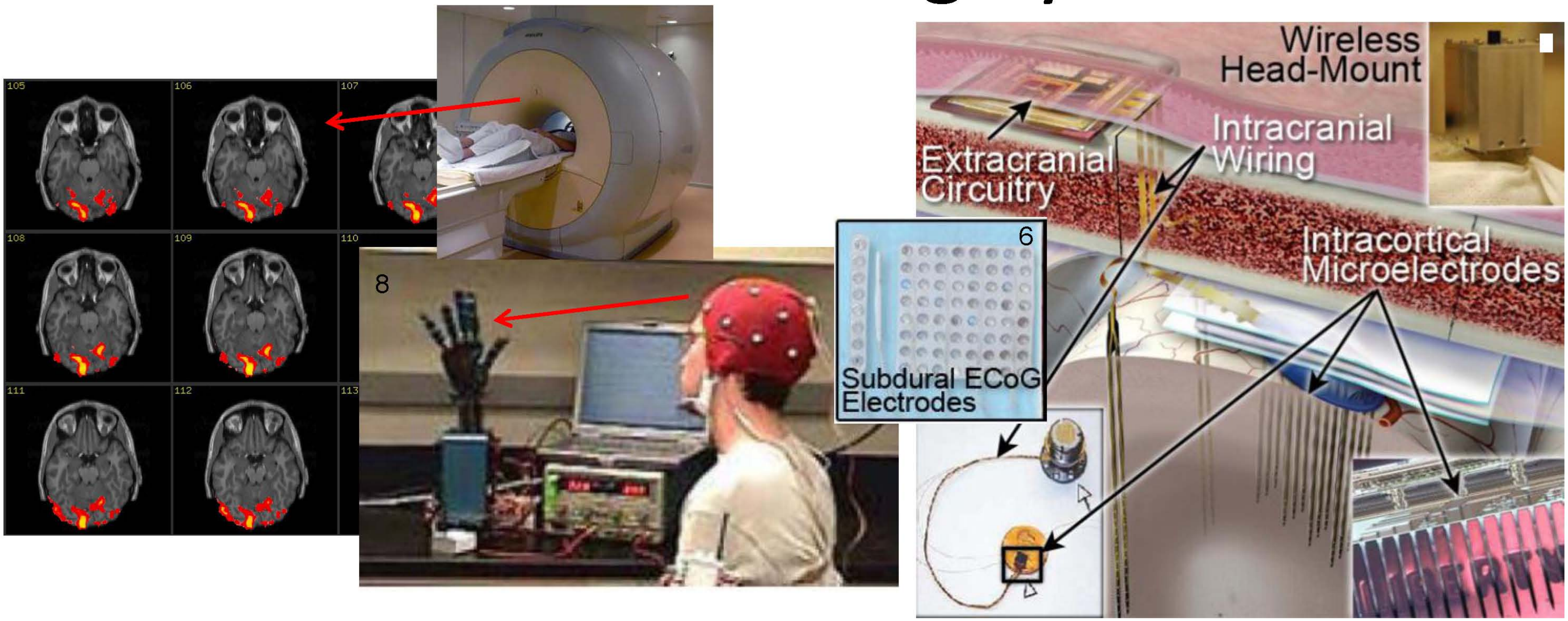

fMRI	Large/expensive	mm (deep)	> s	Hemodynamic	Clinical
NIRS	Portable	~ cm (surface)	< ms	Hemodynamic	Clinical
EEG	Portable	~ cm (surface)	< ms	Electrical / field potentials	Seizure & prosthetics
ECoG	Semi-Invasive	~ mm cortical	< µs	Electrical / spikes & LFPs	Clinical & research[6]
MEA	Invasive	~ 10s of µm	< µs	Electrical / spikes & LFPs	Research[2,4]

fMRI = functional magnetic resonance imaging
NIRS = near infrared spectroscopy
ECoG = electrocorticography
MEA = microelectrode array

Fully Passive Wireless Neurorecorder

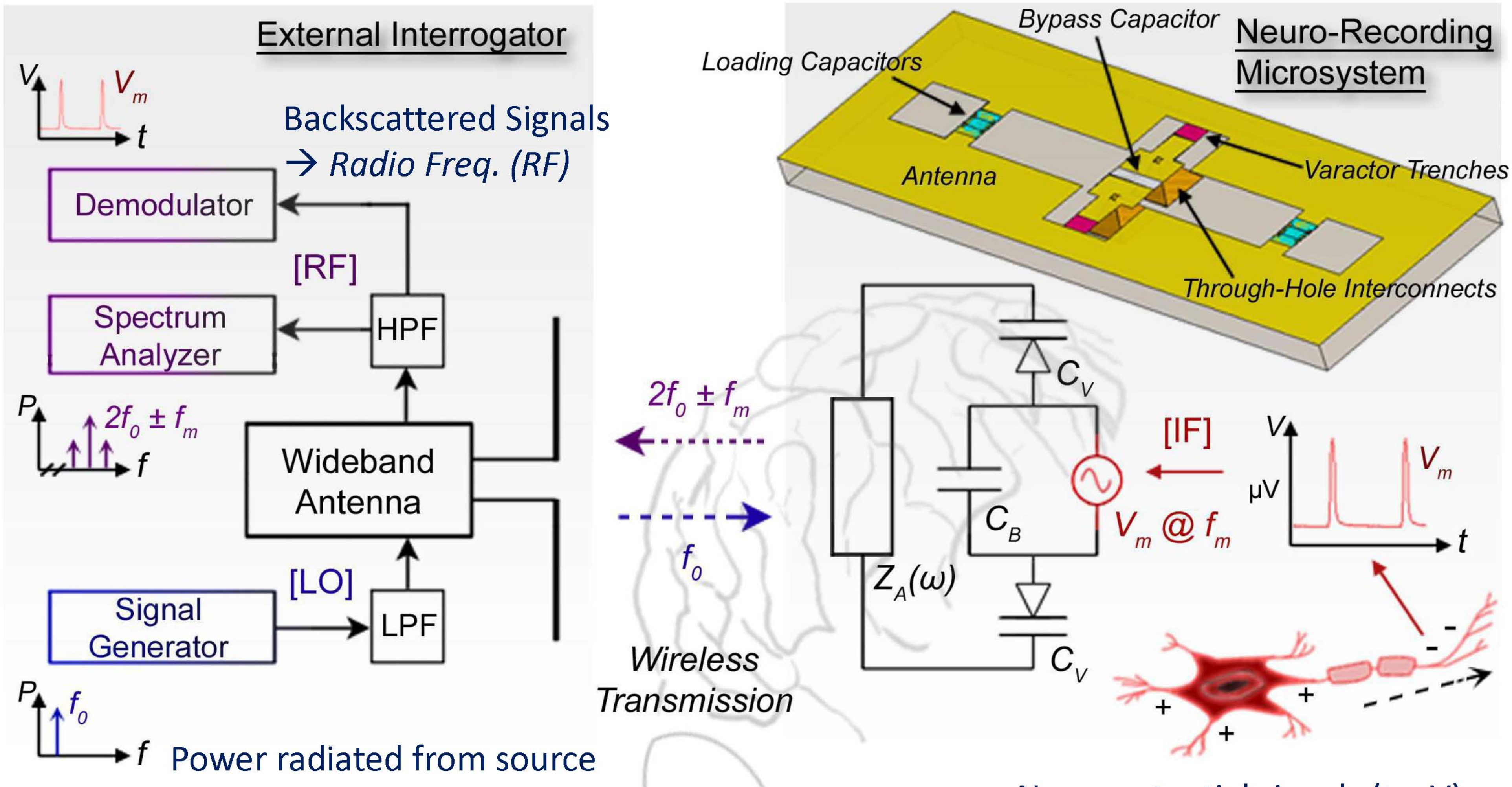

Backscattered Signals
→ *Radio Freq. (RF)*

Power radiated from source or interrogator (~ mW)
→ *Local Oscillator (LO)*

Neuropotential signals (~ μV)
→ *Intermediate Freq. (M or IF)*

Microsystem: Nonlinear Mixer

Nonlinear Mixer → Passive Recording of Neuropotentials (V_m)

$f_{rf} = n \cdot f_0 \pm m \cdot f_m$ ← backscattered RF signal (P_{IM3})

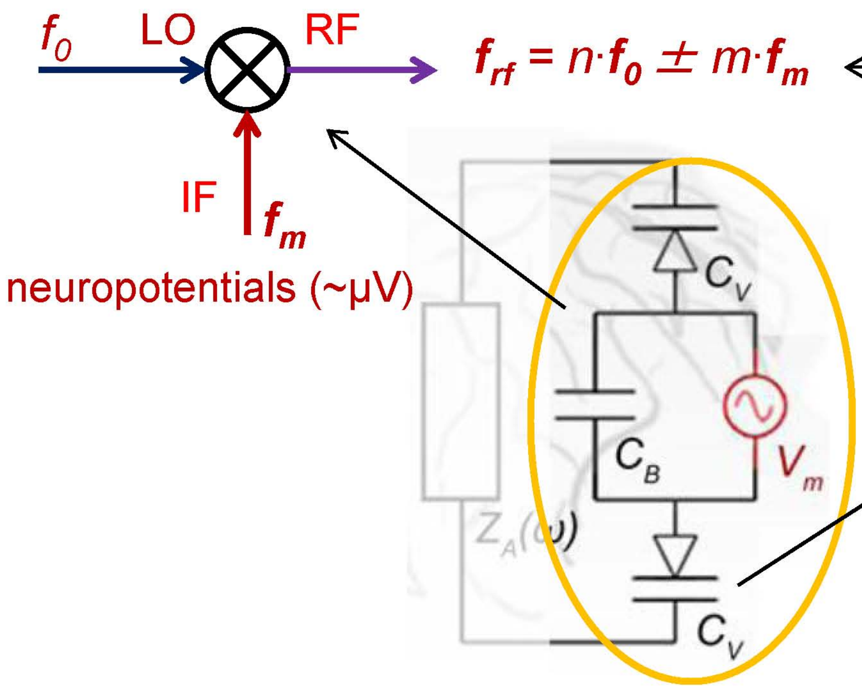

Nonlinear voltage variable capacitance:

$$C_v(V) = \frac{C_j}{(1 - \frac{V}{V_j})^{\gamma}}$$

Mixer Output (Taylor Series Approximation):

$$I = (c_{1a}+c_{3a})\, sin(\omega_0 t) + (c_{1a}+c_{3a})\, sin(\omega_m t) + c_{3b}\, sin(2\omega_0 t \pm \omega_m t) + c_{3b}\, sin(\omega_0 t \pm 2\omega_m t) + \ldots$$

targeted RF backscattered product

Microsystem: Integrated Antenna

Basic Slot Antenna

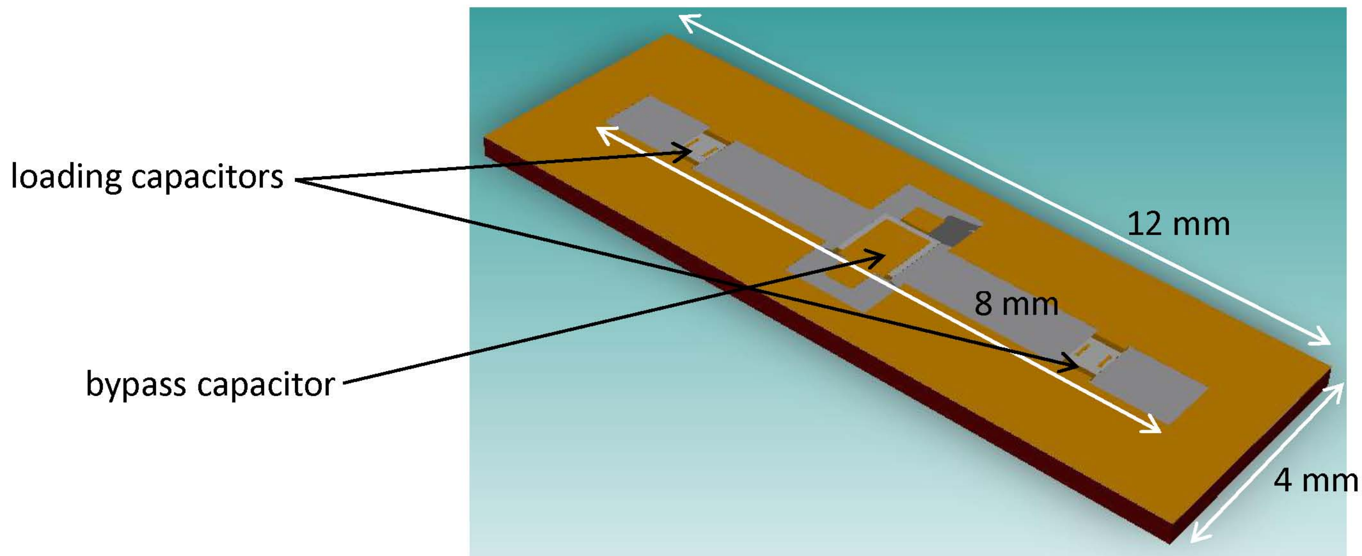

Electrically small antenna → antenna *Gain* limited to ≤ 1.76 dBi

Loading capacitors → tune frequency (dual-band operation @ f_0 & $2f_0 \pm f_m$)

Wireless Backscattering System

Wireless Path Loss in Backscattering System

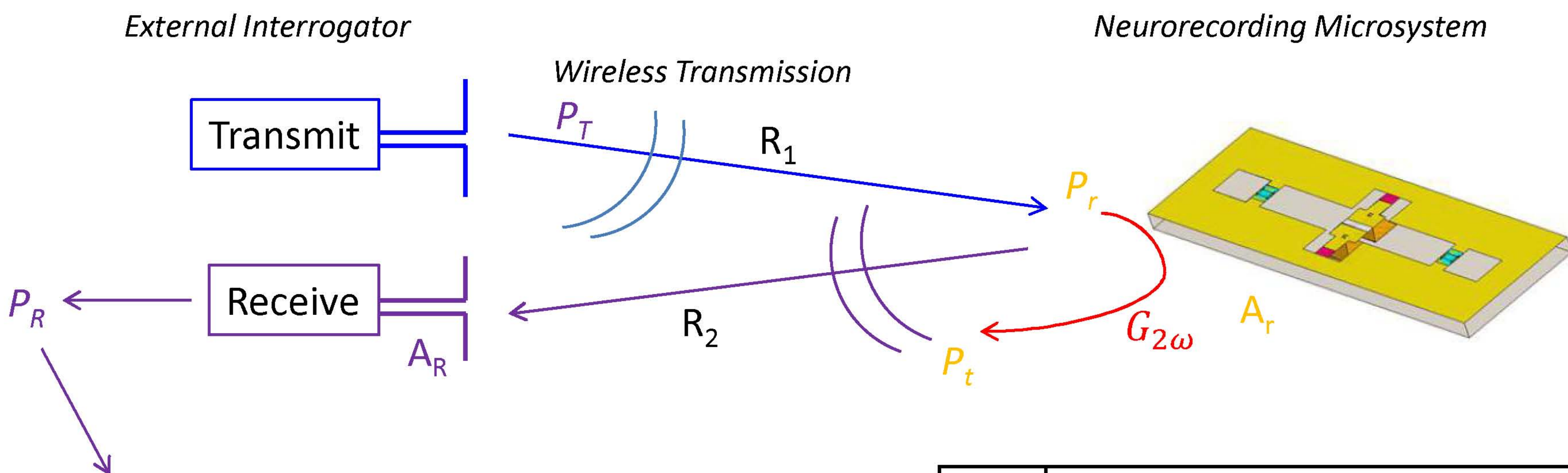

P_{IM3} $(2f_0 \pm f_m)$ Backscattered:

$$P_R = \sigma \frac{P_T G_T}{4\pi {R_1}^2} \cdot \frac{G_t}{4\pi {R_2}^2} \cdot \frac{{\lambda_2}^2}{4\pi} G_R = \sigma \frac{P_T G_T G_t}{(4\pi)^2 R^4} \cdot \frac{\lambda^2}{4\pi} G_R$$

$(R_1 = R_2 = R)$

$$\sigma = 4\pi r^2 \frac{S_t}{S_r} = \frac{{\lambda_1}^2}{4\pi} G_r G_{2\omega} G_t$$

P_T, P_R	Power transmitted/received by external interrogator
G_T, G_R	Gain of external interrogator transmit/receive antenna modes
A_r, A_R	Effective aperture of microsystem/external interrogator antenna ($\lambda^2/4\pi$)
$G_{2\omega}$	Conversion gain of onboard nonlinear mixer
G_t, G_r	Gain of microsystem transmit/receive antenna modes
λ_1, λ_2	Wavelength at f_0 (supply) and $2f_0 \pm f_m$ (backscatter) frequencies

Fabrication

Fabrication Process

Completed Neurorecorder

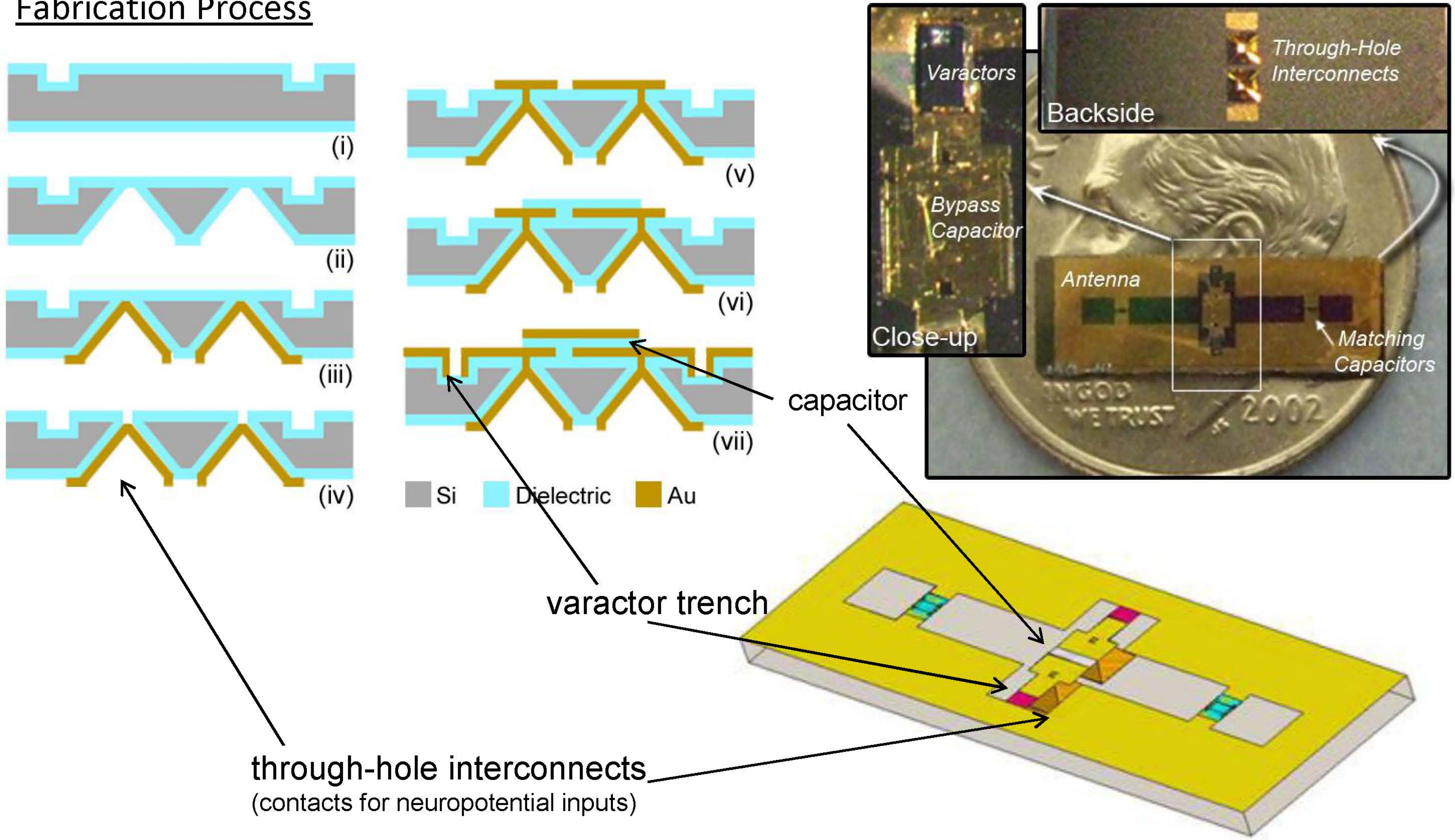

Testing in Air

Testing in "Free-Space" with emulated neuropotentials (V_m) generated via function generator

Measured wirelessly backscattered 3rd order harmonics or $P_{IM3}(2f_0 \pm f_m)$

Spectral Output

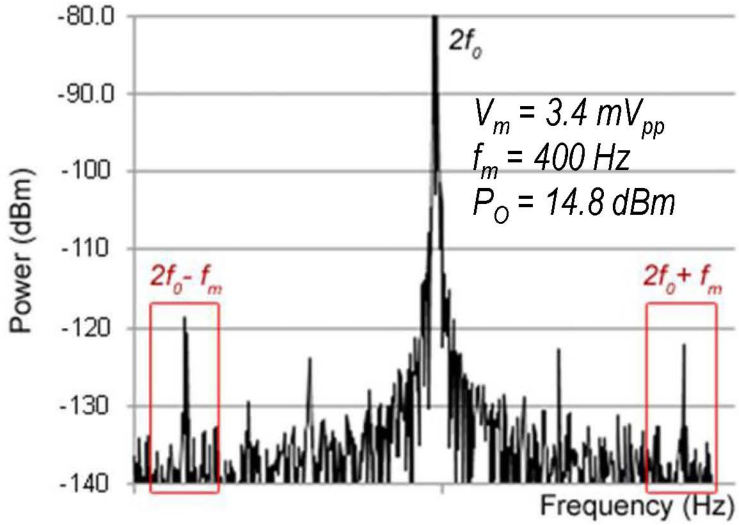

measured by spectrum analyzer

Demodulated Output

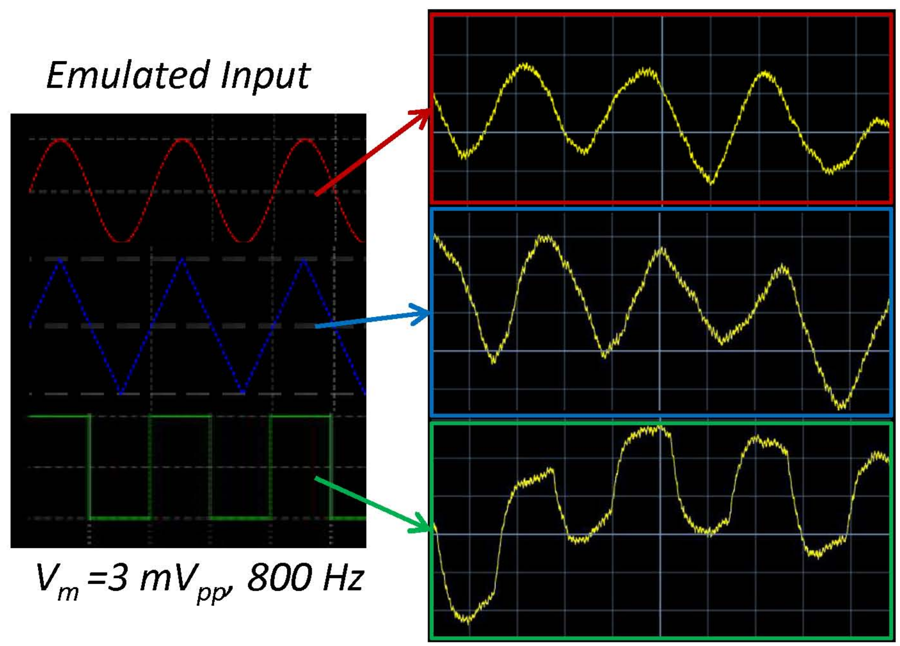

after synchronous AM demodulation

Testing with Frog

Wireless Recording from Sciatic Nerve

Setup Procedure

Stimulate (inject current) higher end of nerve

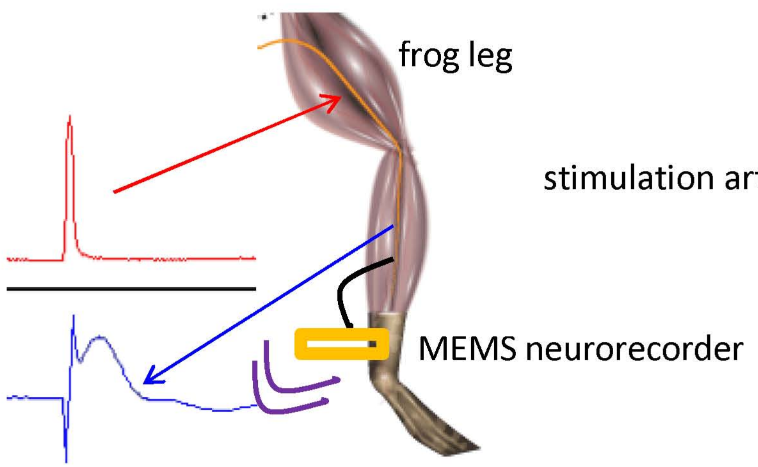

Wirelessly record CAPs

Wired & Wireless Measurements

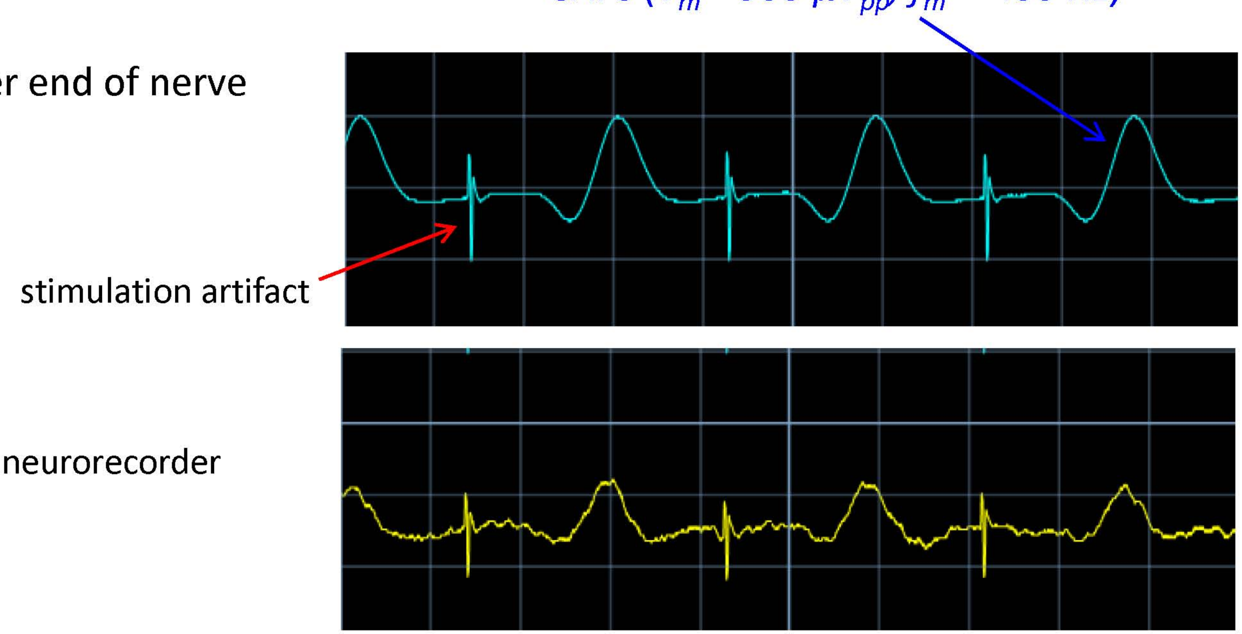

Used signal averaging on oscilloscope to improve SNR by around 11.3dB

CAPs = Compound Action Potentials (integration of many propagating action potentials/spikes in nerve bundle)

Summary of Measurements in Air

Footprint	*Dimensions*	12×4×0.5 mm^3
Detected Input Signals	*Bandwidth*	5 – 3000 Hz
	Amplitude	≥ 500 μV_{pp}
	Distance	≤ 1.5 cm
RF Transmission	*Radiated Power*	≤ 16.7 dBm (47 mW)
	Frequency	2.2 – 2.45 GHz
RF Reception	*Sideband Level*	≤ -97 dBm (for V_m = 50 mV_{pp})
	Noise Floor	≈ -136 dBm
	Frequency	4.4 – 4.9 GHz
Thermal Characteristics	*Temperature Rise*	≤ 0.15 ± 0.1°C
	SAR (estimated)	≤ 0.112 W/kg

Wireless Testing in Phantom Mimicking Real Head Tissues

Final Goal – Implantable Wireless System in Lossy & Inhomogeneous/Stratified Tissue Media

(until now wireless testing in air only)

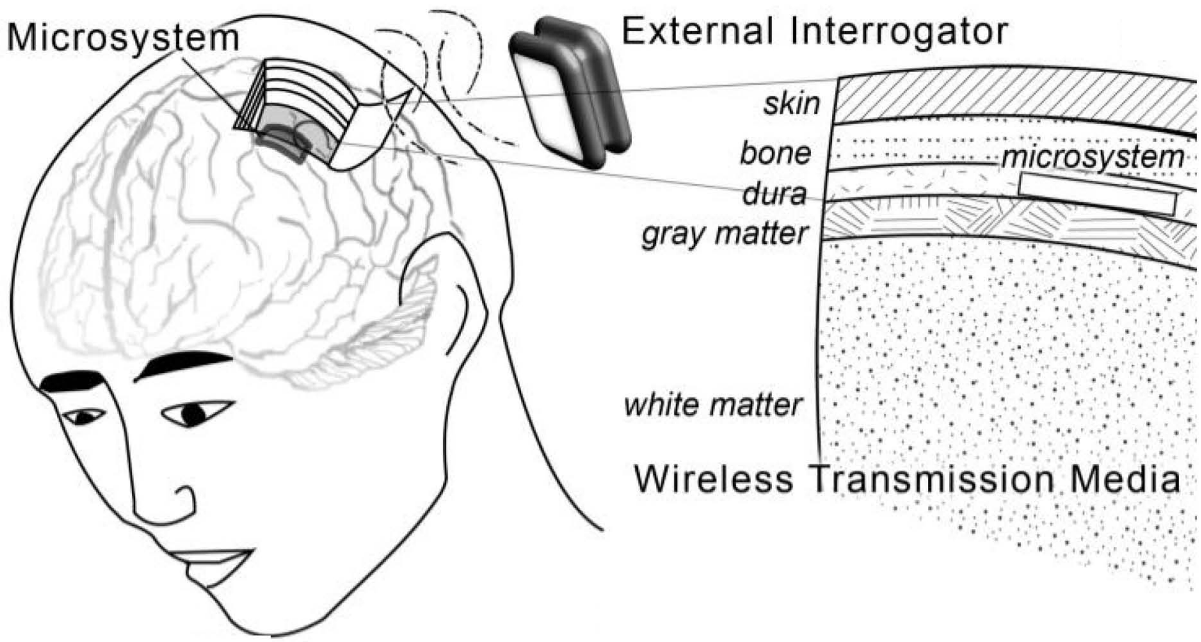

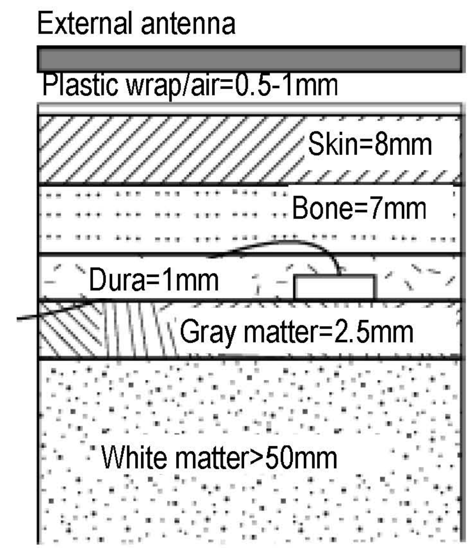

Phantom Preparation

Semisolid phantoms made for each head layer[23]

Measure dielectric properties

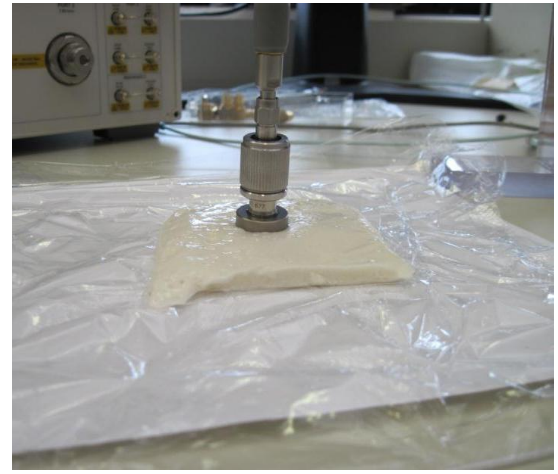

Symbols = real meas.[23-24]

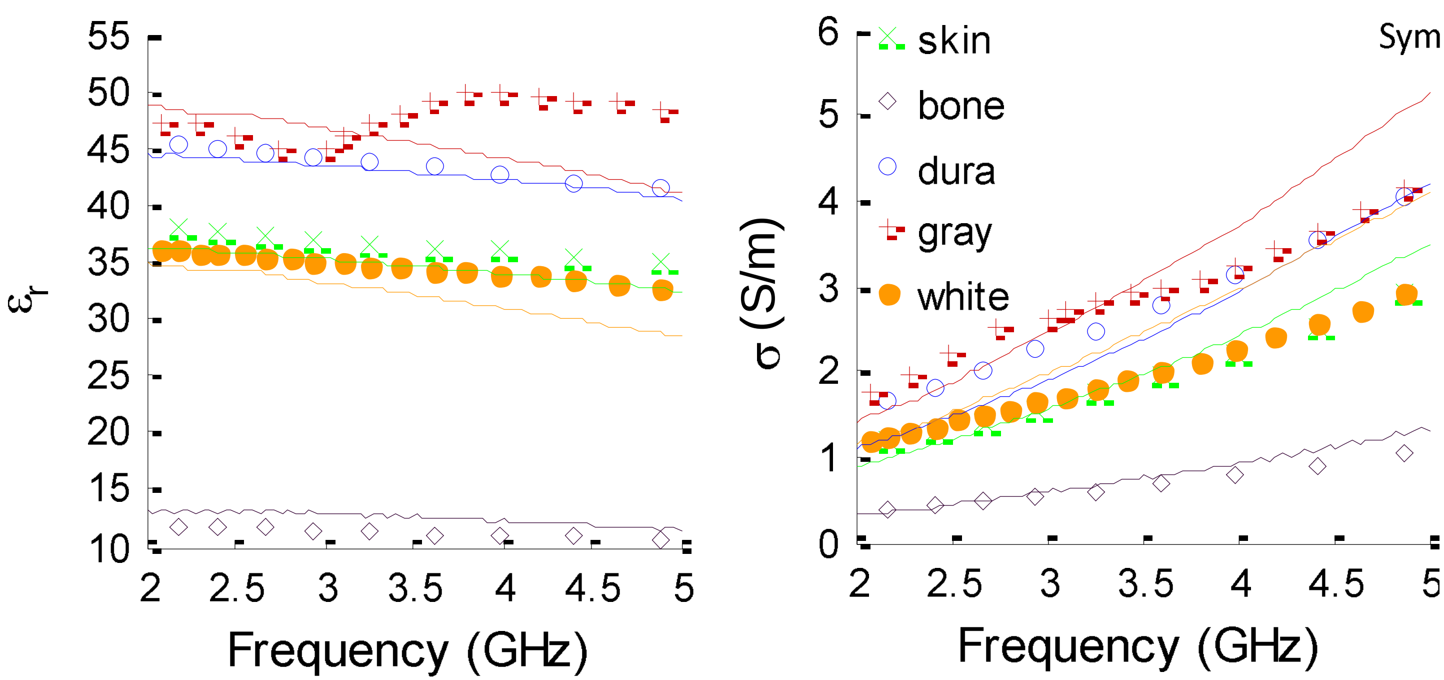

Phantom Media Testing

MEMS neuro-recorder (parylene coated)

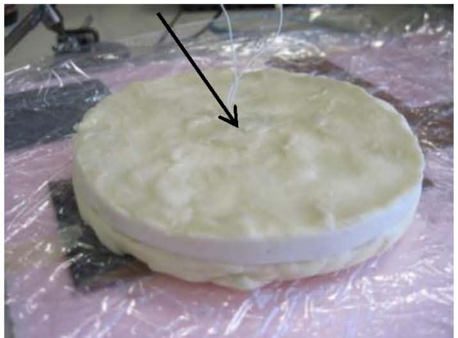

scalp/skull/dura

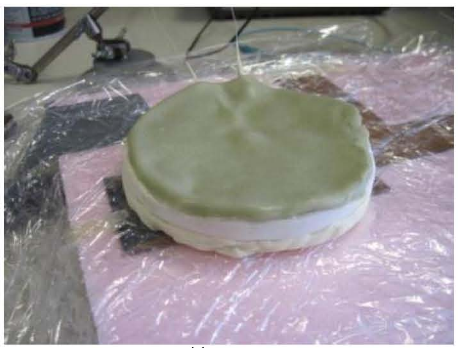

gray matter

complete phantom

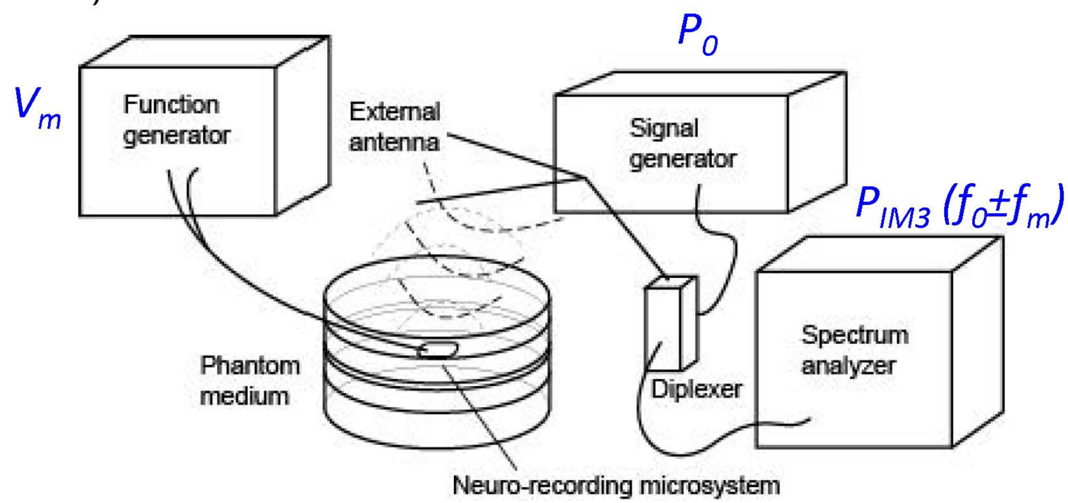

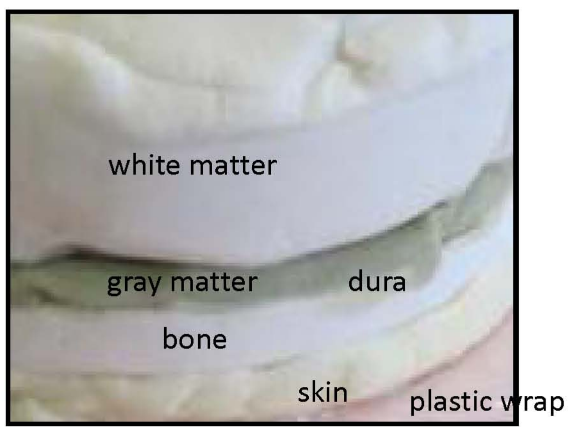

implant depth ~ 1.5 cm (dura)

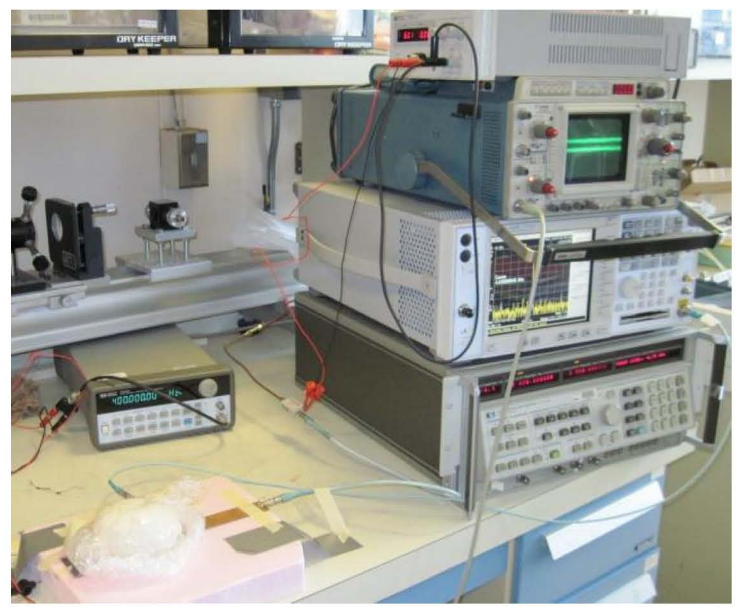

Phantom Media Testing

Measurements of Neurorecorders in Phantom

Comparison of glass & silicon substrates

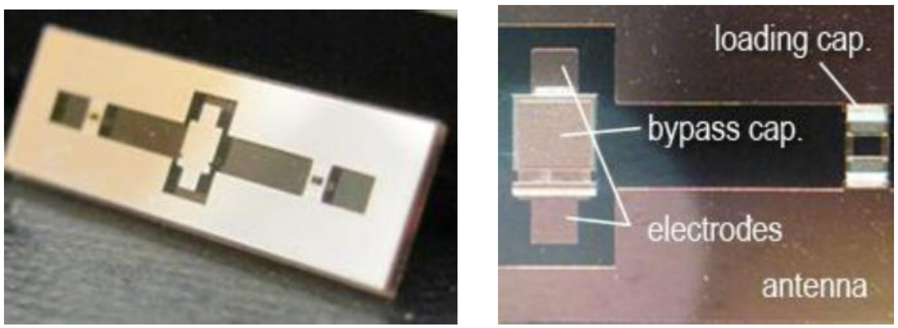

Low Resistivity Si	0	**0**
High Resistivity Si	38.9	**22.0**
Glass	**36.6**	**21.3**

Skin depth accounts for real losses in phantom

$$\delta = \frac{1}{Im\left[\sqrt{\omega\mu(\omega\hat{\varepsilon} - j\sigma)}\right]} = \frac{1}{Im\left[\sqrt{\omega^2\mu\varepsilon' - j\omega\mu(\omega\varepsilon'' + \sigma)}\right]}$$

Spectral Output

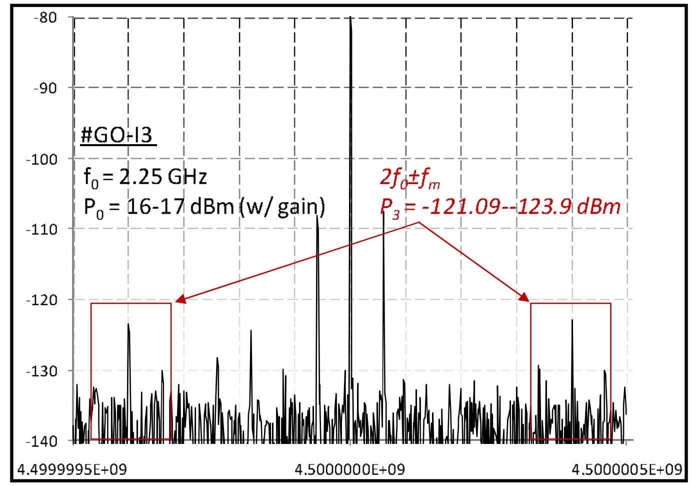

Ratio of P_{IM3} (received) to P_0 (supplied)

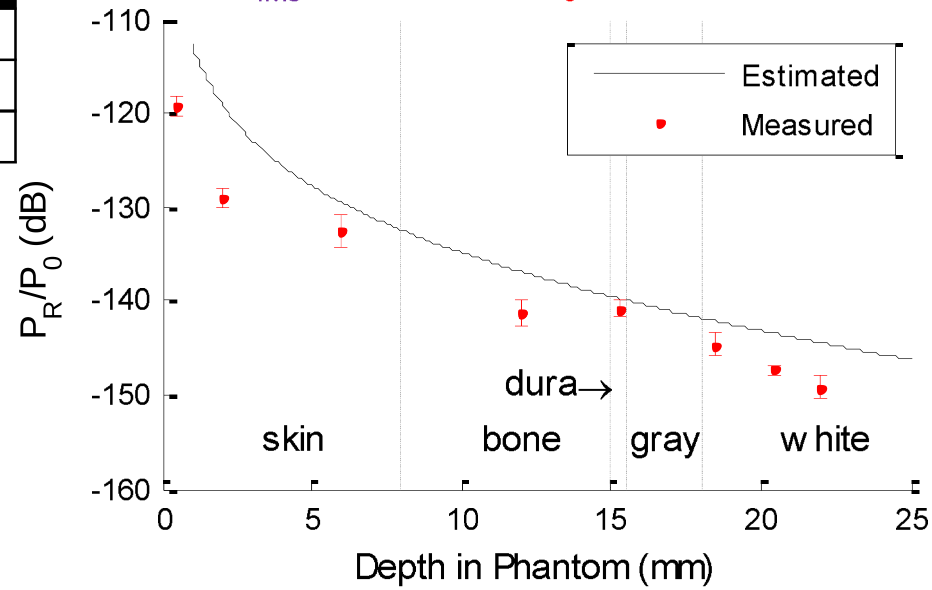

Conclusion & Future Work

Conclusion:

		In Air	
Detected V_m	*Amplitude*	≥ 500 μV_{pp}	
RF Transmission	*Radiated Power*	≤ 16.7 dBm (47 mW)	
	Frequency	2.2 – 2.45 GHz	
RF Reception	P_{IM3} (V_m=50mV_{pp})	≤ -97 dBm	
	Noise Floor	≈ -134 dBm	
Thermal Characteristics	*Temperature Rise*	≤ 0.15 ± 0.1°C	
	SAR	--	

Future Work:

-Thermal characterization of neurorecorder in phantom

-Increasing sensitivity (minimum detectable V_m)

→ Increasing nonlinearity (γ) of varactors

→ Increasing SNR of external interrogator (lowering phase noise)

References

1) M.A.L. Nicolelis, *Methods for Neural Ensemble Recordings.* 2nd Ed. CRC Press, 2008.
2) A.V. Nurmikko, et al., "Listening to Brain Microcircuits for Interfacing With External World—Progress in Wireless Implantable Microelectronic Neuroengineering Devices," Proceedings of the IEEE 98(3), 375-388, March 2010.
3) L.R. Hochberg, et al., "Neuronal ensemble control of prosthetic devices by a human with tetraplegia," Nature 442, 164-171, 2006.
4) K.D. Wise, et al., "Microelectrodes, microelectronics, and implantable neural microsystems," IEEE Proceedings, vol. 96, no. 7, pp. 1184-1202 Jul. 2008.
5) D.R. Kipke, et al. "Advanced Neurotechnologies for Chronic Neural Interfaces: New Horizons and Clinical Opportunities," J. Neuroscience, 12, vol. 28, no. 46, 11830-11838, Nov. 2008.
6) J.P. Blount, et al., "Advances in intracranial monitoring," Neurosurg. Focus 25 (3):E18, 1-8, Sept. 2008.
7) R.R. Harrison, "Design of integrated circuits to observe brain activity," *IEEE Proceedings*, vol. 96, no.7, pp. 1203-1216, Jul. 2008.
8) M. Mollazadeh, et al. "Wireless Multichannel Acquisition of Neuropotentials," in Biomedical Circuits and Systems Conference, Nov. 2008 (BioCAS), 49-52.
9) Y.K. Song, et al., "Active microelectronic neurosensor arrays for implantable brain communication interfaces," IEEE Transactions in Neural Systems and Rehabilition Engineering, vol. 17, no. 4, pp. 339-345, June 2009.
10) C. Constantinescu."Trends and Challenges in VLSI Circuit Reliability," IEEE Micro Magazine, 14-19, 2003.
11) Y. Li, et al. "Overcoming Early-Life Failure and Aging for Robust Systems," IEEE Design and Test of Computers, 28-39, 2009.
12) A. Waziri, et al., "Initial surgical experience with a dense cortical microarray in epileptic patients undergoing craniotomy for subdural electrode implantation," Neurosurgery, 64(3), 540–545, March 2009.
13) S. Kim *et al.*, "Thermal impact of an active 3-d microelectrode array implanted in the brain," *IEEE Trans. Neural Sys. Rehab. Eng.*, vol. 15, no. 4, pp. 493-501, 2007.
14) D. L. Means and K. W. Chan, "Evaluating compliance with FCC guidelines for human exposure to radiofrequency electromagnetic fields," *FCC Office of Engineering and Technology OET*, bulletin 65, supplement C, 2001.
15) B.C. Towe, "Passive backscatter biotelemetry for neural interfacing," Proc. *IEEE-EMBS Int. Conf. Neural Eng.*, May 2007, pp. 144-147.
16) A. Abbaspour-Tamijani, M. Farooqui, B.C. Towe, and J. Chae, "A miniature fully-passive microwave back-scattering device for short-range telemetry of neural potentials," *Proc. Ann. Int. Conf. IEEE-EMBS*, Aug. 2008, pp. 129-132.
17) C.A. Balanis, *Advanced Engineering Electromagnetics.* Hoboken, NJ: John Wiley & Sons, 1989.
18) J. Galejs, *Antennas in Inhomogeneous Media.* London, Great Britain: Pergamon Press, 1969.
19) S.A. Maas, *Nonlinear Microwave and RF Circuits.* Norwood, MA: Artech House, 2003
20) C.A. Balanis, *Antenna Theory: Analysis and Design.* Hoboken, NJ: John Wiley & Sons, 2005.
21) H.A. Wheeler, "Fundamental limitations of small antennas," *IEEE Proceedings of the Institute of Radio Engineers*, pp. 1479-1484, March 1947.
22) R.F. Harrington, "Effect of antenna size on gain, bandwidth, and efficiency," *Journal of Research of the National Bureau of Standards—D , Radio Propagation*, vol. 64D, no. 1, pp. 1-12, Jan. 1960.
23) K. Ito, K. Furuya, Y. Okano, and L. Hamada, "Development and characteristics of a biological tissue-equivalent phantom for microwaves." Electronics and Communications in Japan (Part I: Communications), vol. 84, pp. 67–77, 2001.
24) C. Gabriel, and S. Gabriel, "Compilation of the dielectric properties of body tissues at RF and microwave frequencies," *Report for Armstrong Laboratory (AFMC), Occupational and Environmental Health Directorate, Radiofrequency Radiation Division: AL/OE-TR-1996-0037, TX, USA,* 1996.
25) K.S. Cole, and R.H. Cole, "Dispersion and absorption in dielectrics," *Journal of Chemical Physics,* vol. 9, pp. 341–52, Apr. 1941.
26) D. L. Means and K. W. Chan, "Evaluating compliance with FCC guidelines for human exposure to radiofrequency electromagnetic fields," *FCC Office of Engineering and Technology OET,* bulletin 65, supplement C, 2001.
27) J.C. LaManna, et al., "Stimulus-Activated Changes in Brain Tissue Temperature in the Anesthetized Rat", *Metabolic Brain Disease*, Vol. 4, pp. 225-237, 1989.
28) T. Fujii and Y. Ibata, "Effects of heating on electrical activities of guinea pig olfactory cortical slices," *Eur. J. Physiol.*, vol. 392, pp. 257–260, 1982.
29) M. Ueda, J. Bures, and J. Fischer, "Spreading depression elicited by thermal effects of ultrasonic irradiation of cerebral cortex in rats," *J. Neurobiol.*, vol. 8, pp. 381–393, 1977.
30) H.N. Schwerdt, W. Xu, S. Shekhar, A. Abbaspour-Tamijani, B.C. Towe, F.A. Miranda, and J. Chae, "A fully passive wireless microsystem for recording of neuropotentials using RF backscattering methods," IEEE J. MEMS, vol. 20, no. 5, pp. 1119-1130, Oct. 2011.
31) H.N. Schwerdt, F.A. Miranda, and J. Chae, "A Fully Passive Wireless Backscattering Neuro-Recording Microsystem Embedded in Dispersive Human Head Phantom Medium," IEEE Electron Device Letters, vol. 33, no. 6, pp. 908-910, June 2012.

Acknowledgement

This work was supported by:

National Science Foundation (NSF) (#ECCS-0702227)

National Institutes of Health (NIH) (#5R21NS059815-02)

NASA Graduate Student Research Program (GSRP) Fellowship (#NNX09AK93H)

Appendix I: Thermal Impact

Fully Passive Wireless Microsystem ΔT vs Wireless RF P_0 Supplied (in air & @25°C)

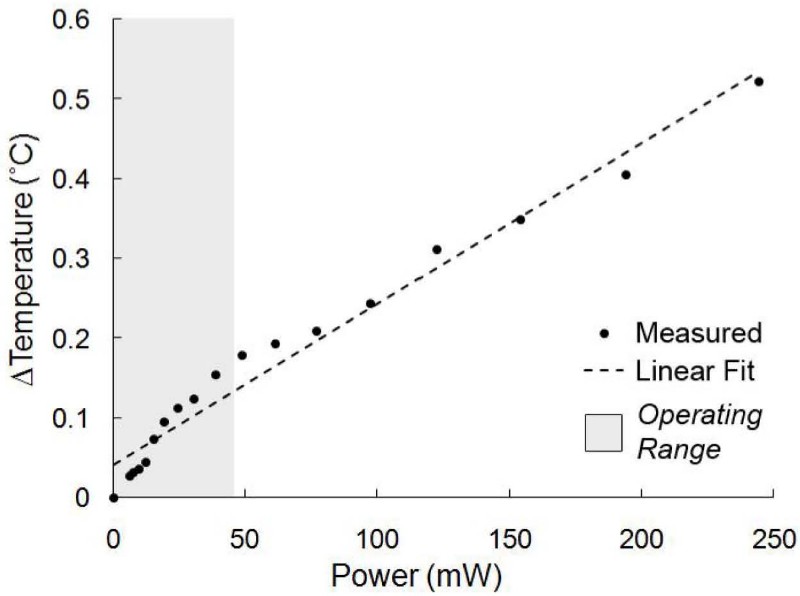

Utah Electrode Array ΔT vs P Dissipated

(No wireless link for this study)

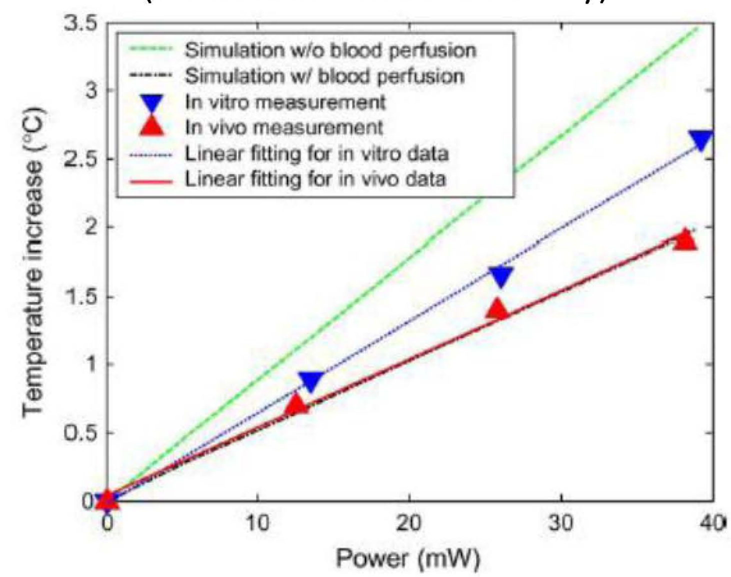

P can range up 40 mW, but if kept at 13 mW, ΔT=0.38°C

ΔT > 1 °C → long-term effects on the brain tissue [20].

ΔT > 2 °C → aberrant activity in brain (as shown in guinea pig olfactory cortical slices) [21]

ΔT > 3 °C → physiological abnormalities and tissue death (cortical spreading depression was observed by heating the cortex of anesthetized rats by 3.4°C) [22]

Appendix II(a): Varactor Mixer

$$C(V) = \frac{C_j}{(1 - \frac{V}{V_j})^{\gamma}}$$

Input:

$$V = V_0 cos(\omega_0 t) + V_m cos(\omega_m t)$$

Output (Taylor Series Approx.): $I = \frac{d}{dt}\left(\sum_{n=1}^{\infty} c_n V^n\right) V$ $\quad I = \frac{d}{dt}(c_1 + c_2 V + c_3 V^2 + \ldots)V$

$$I = (c_{1a}+c_{3a})\, sin(\omega_0 t) + (c_{1a}+c_{3a})\, sin(\omega_m t) + c_{2a1}\, sin(2\omega_0 t) + c_{2b}\, sin(2\omega_m t) + c_{2c1}\, sin(\omega_0 t \pm \omega_m t) + c_{3b}\, sin(2\omega_0 t \pm \omega_m t) + c_{3b}\, sin(\omega_0 t \pm 2\omega_m t) + \ldots$$

$$c_{3b} = \frac{-C_j(\gamma^2 + \gamma)}{V_j^{\,2}} \cdot \left(\frac{V_0^2 V_m(\omega_m)}{4} + \frac{V_0 V_m(V_0\omega_0 + V_m\omega_m)}{2}\right)$$

Targeted backscattered signals

Back to Back Config. : $I = \frac{d}{dt}\left(\sum_{n=1}^{\infty} c_n V_+^{n+1} - c_n V_-^{n+1}\right)$

$$I = \frac{d}{dt}(c_1 V_+ - c_1 V_- + c_2 V_+^2 - c_2 V_-^2 + c_3 V_+^3 - c_3 V_-^3 + \cdots)$$

$$I = (c_{1a}+c_{3a})\, sin(\omega_0 t) + (c_{1a}+c_{3a})\, sin(\omega_m t) + c_{3b}\, sin(2\omega_0 t \pm \omega_m t) + c_{3b}\, sin(\omega_0 t \pm 2\omega_m t) + \ldots$$

Appendix II(b): Varactor Mixer

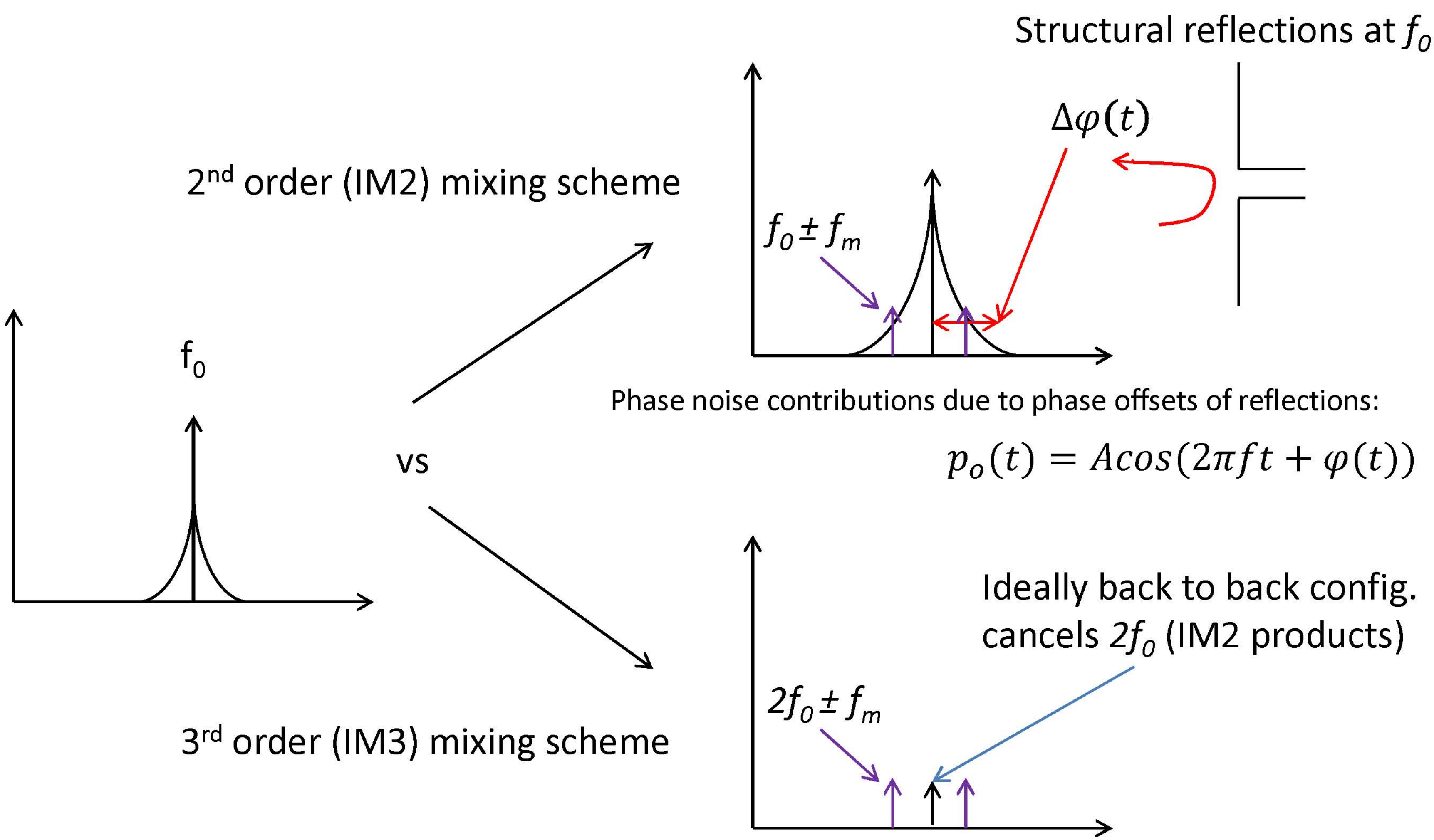

Appendix III: Backscattering Link

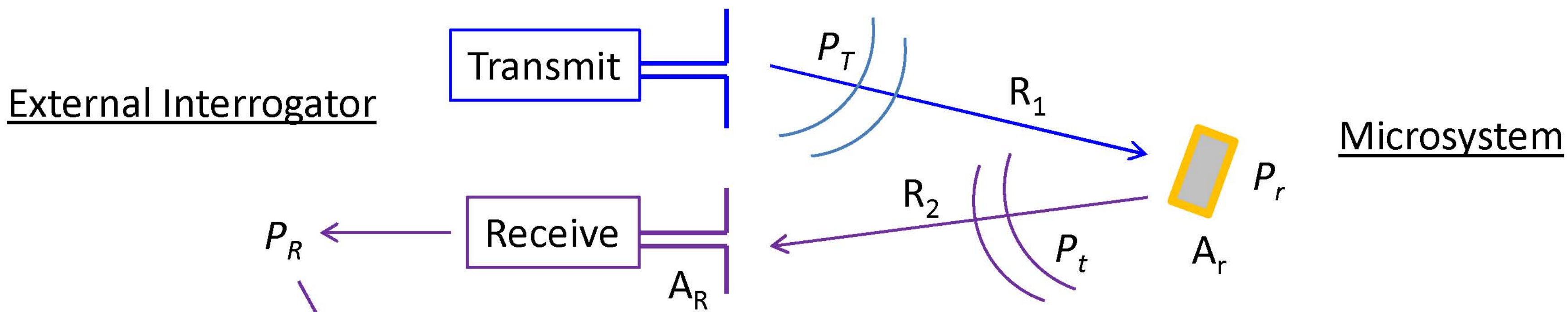

Microsystem receive:

$$P_r = S_T A_r$$

$$P_r = \frac{P_T G_T}{4\pi {R_1}^2} \cdot \frac{{\lambda_1}^2}{4\pi} G_r$$

Microsystem transmit:

$$P_t = P_r G_{2\omega} G_t$$

$$P_t = \sigma \frac{P_T G_T}{4\pi {R_1}^2}$$

$$\sigma = 4\pi r^2 \frac{S_t}{S_r} = \frac{{\lambda_1}^2}{4\pi} G_r G_{2\omega} G_t$$

External Interrogator receive (backscattered power):

$$P_R = S_t A_R$$

$$P_R = \frac{P_t G_t}{4\pi {R_2}^2} \cdot \frac{{\lambda_2}^2}{4\pi} G_R$$

$$P_R = \frac{P_T G_T}{4\pi {R_1}^2} \cdot \frac{{\lambda_1}^2}{4\pi} G_r \cdot \frac{G_t}{4\pi {R_2}^2} \cdot \frac{{\lambda_2}^2}{4\pi} G_R G_{2\omega} G_t$$

$$P_R = \sigma \frac{P_T G_T}{4\pi {R_1}^2} \cdot \frac{G_t}{4\pi {R_2}^2} \cdot \frac{{\lambda_2}^2}{4\pi} G_R$$

Appendix IV: ADS Circuit Simulations

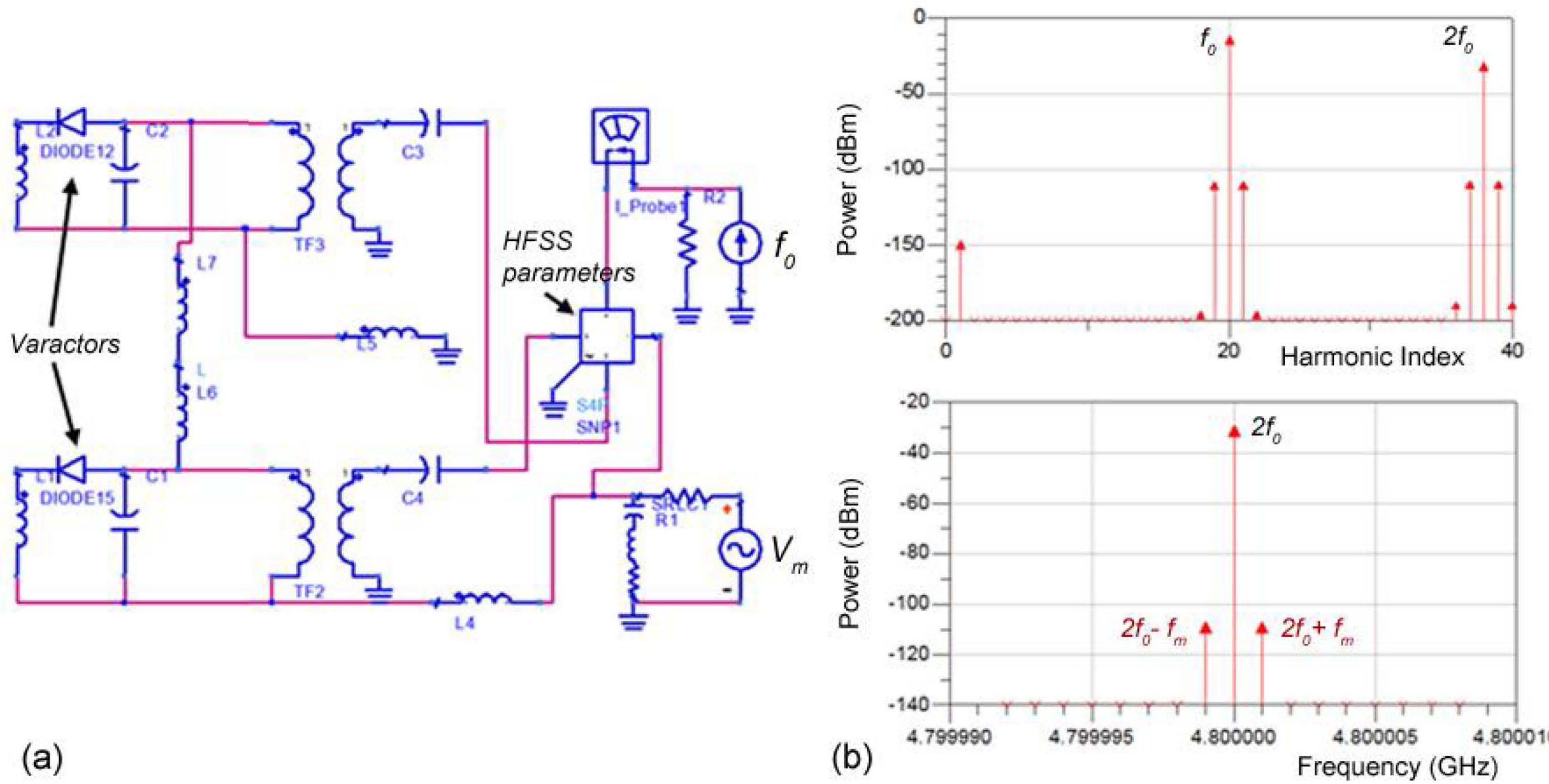

Simulated backscattering spectral response with V_m of 100 μV_{pp} sinusoidal at f_m (IF) of 1 kHz, incident radiated power, P_0, of 1 mW (0 dBm) at f_0 of 2.4 GHz.

Appendix IV(b): Detailed ADS

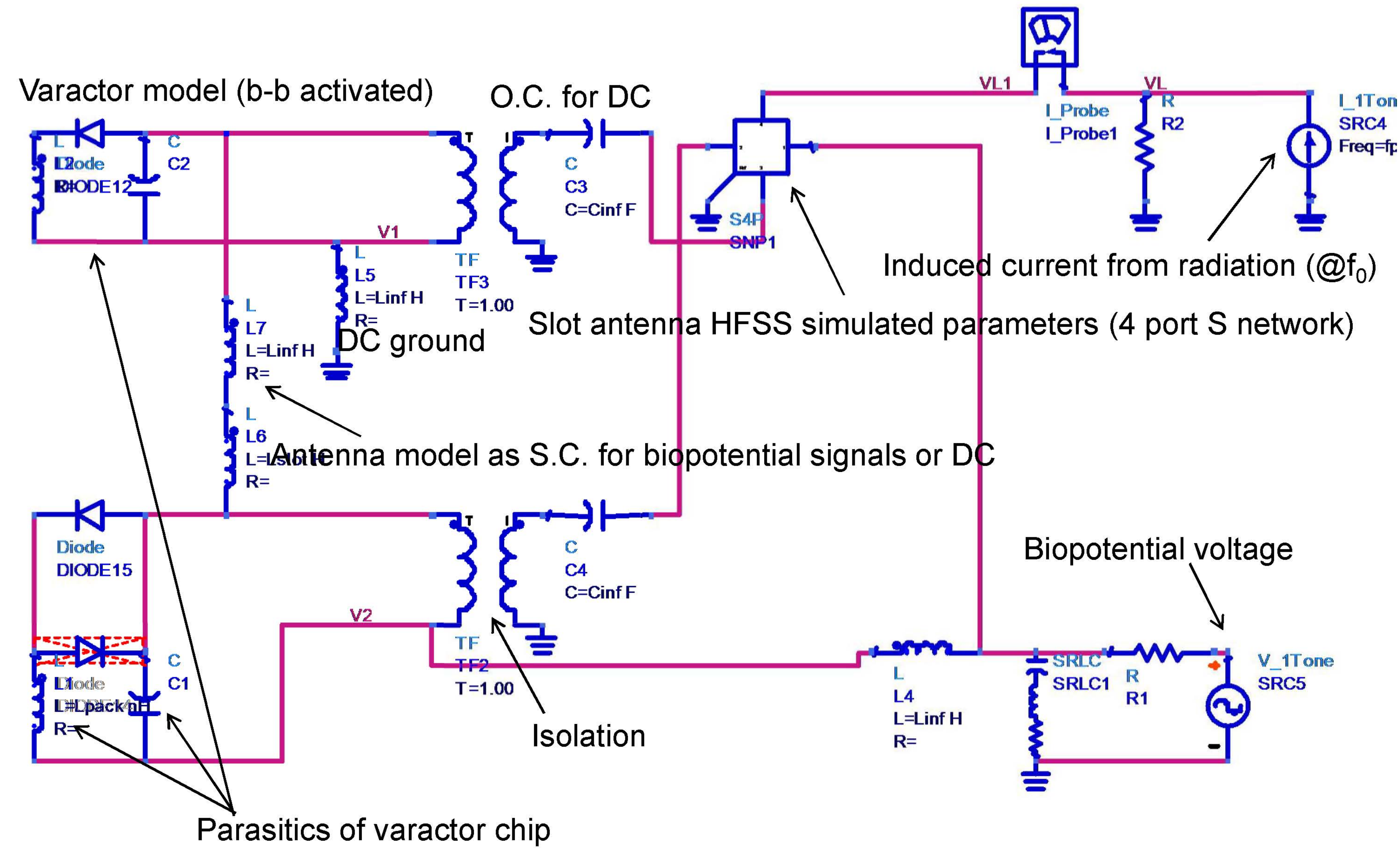

Appendix V: Demodulator

Simplified Block Diagram

Signal Generator

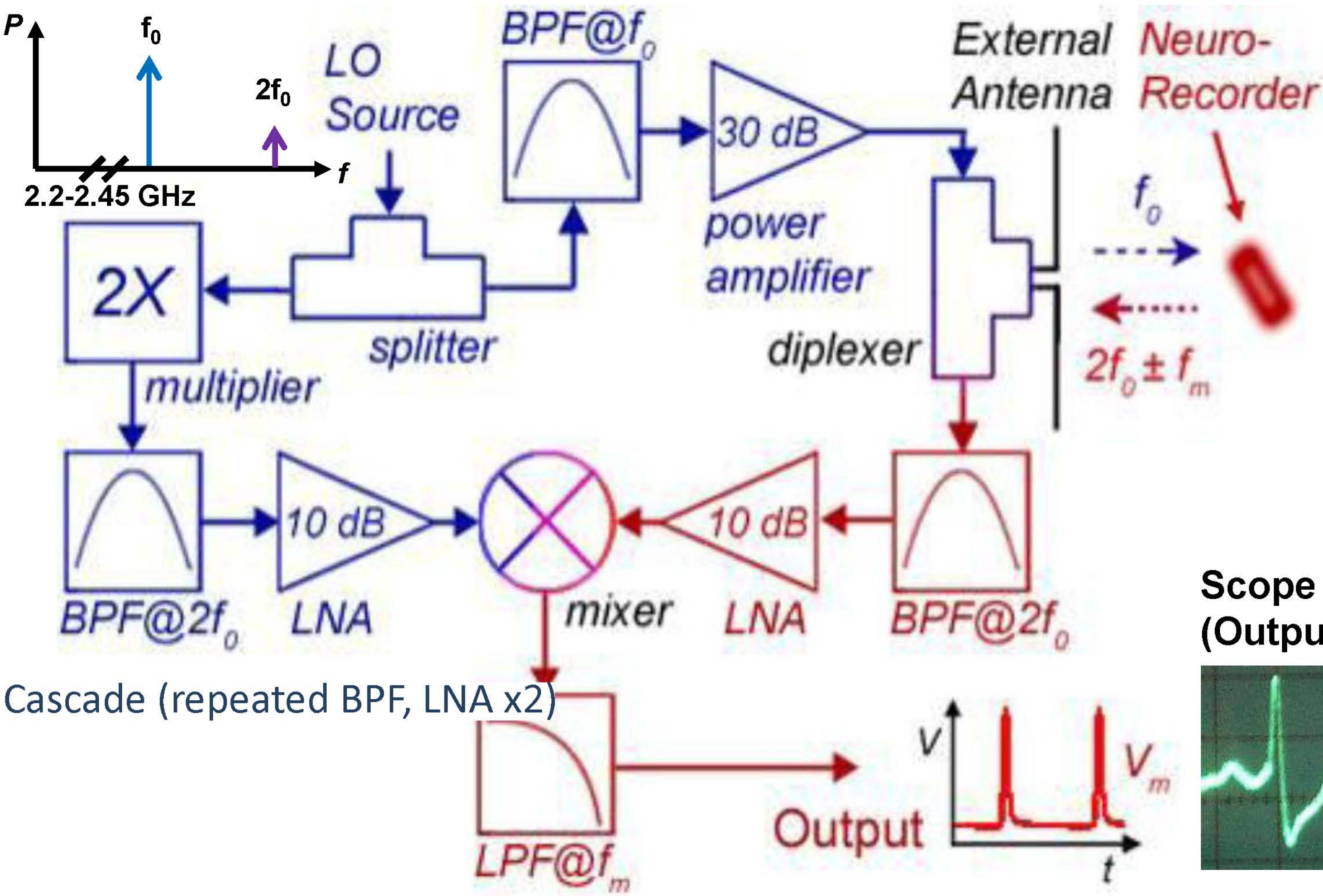

MEMS Device

Cascade (repeated BPF, LNA x2)

Variable gain amplification & filtering

Scope (Output Waveforms)